EUROPEAN SYNCHROTRON RADIATION FACILITY

INSTALLATION EUROPEENNE DE RAYONNEMENT SYNCHROTRON

Experiment Report Form

The double page inside this form is to be filled in by all users or groups of users who have had access to beam time for measurements at the ESRF.

Once completed, the report should be submitted electronically to the User Office via the User Portal:
https://wwws.esrf.fr/misapps/SMISWebClient/protected/welcome.do

Deadlines for submission of Experimental Reports

Experimental reports must be submitted within the period of 3 months after the end of the experiment.

Experiment Report supporting a new proposal ("relevant report")

If you are submitting a proposal for a new project, or to continue a project for which you have previously been allocated beam time, you must submit a report on each of your previous measurement(s):

- even on those carried out close to the proposal submission deadline (it can be a *"preliminary report"),*
- even for experiments whose scientific area is different form the scientific area of the new proposal,
- carried out on CRG beamlines.

You must then register the report(s) as "relevant report(s)" in the new application form for beam time.

Deadlines for submitting a report supporting a new proposal

- 1st March Proposal Round - **5th March**
- 10th September Proposal Round - **13th September**

The Review Committees reserve the right to reject new proposals from groups who have not reported on the use of beam time allocated previously.

Reports on experiments relating to long term projects

Proposers awarded beam time for a long term project are required to submit an interim report at the end of each year, irrespective of the number of shifts of beam time they have used.

Published papers

All users must give proper credit to ESRF staff members and proper mention to ESRF facilities which were essential for the results described in any ensuing publication. Further, they are obliged to send to the Joint ESRF/ ILL library the complete reference and the abstract of all papers appearing in print, and resulting from the use of the ESRF.

Should you wish to make more general comments on the experiment, please note them on the User Evaluation Form, and send both the Report and the Evaluation Form to the User Office.

Instructions for preparing your Report

- fill in a separate form for each project or series of measurements.
- type your report in English.
- include the experiment number to which the report refers.
- make sure that the text, tables and figures fit into the space available.
- if your work is published or is in press, you may prefer to paste in the abstract, and add full reference details. If the abstract is in a language other than English, please include an English translation.

ESRF	**Experiment title:** Transformation-induced plasticity in zirconia-based ceramics: an in situ microLaue experiment during compression of micropillars	**Experiment number:** A32-2-851
Beamline: BM32	**Date of experiment:** from: 09/11/2022 to: 14/11/2022	**Date of report:** 09/01/2023
Shifts:	**Local contact(s):** MICHA Jean-Sebastien, ROBACH Odile, PURUSHOTTAM RAJ PUROHIT Ravi Raj Purohit	*Received at ESRF:*

Names and affiliations of applicants (* indicates experimentalists):

THOMAS, Olivier; CORNELIUS, Thomas; DASSONNEVILLE, Solène – Aix Marseille Univ, CNRS, IM2NP UMR 7334, Campus de St-Jérôme

CHEVALIER, Jérôme; DEMETRIO DE MAGALHAES, Marcelo – Université de Lyon, INSA-Lyon, UMR CNRS 5510 MATEIS

RODNEY, David – Institut Lumière Matière, CNRS-Université Claude Bernard Lyon 1

Report:

The martensitic transformation of 12 mol% ceria-doped tetragonal zirconia micropillars (MPs) was followed by *in-situ* compression combined with Laue microdiffraction at the BM32 beamline. To perform it, the following proceedings were done ahead of the experiment:

First, 12 mol% ceria-doped zirconia pellets were sintered at 1600 ºC for 10 hours dwell time. The high temperature and sintering time were used to facilitate the growth of large grains with sizes of up to 8 µm needed for the subsequent micro-machining of single-crystalline micropillars. Electron back-scattered diffraction (EBSD, Symmetry, Oxford Instruments) was performed after cutting the pellets into triangular-shaped pieces, and preparing the surface with low-energy milling (Ilion II, Gatan), reducing surface damage and preventing premature phase transformation. These steps are summarized in Fig. 1.

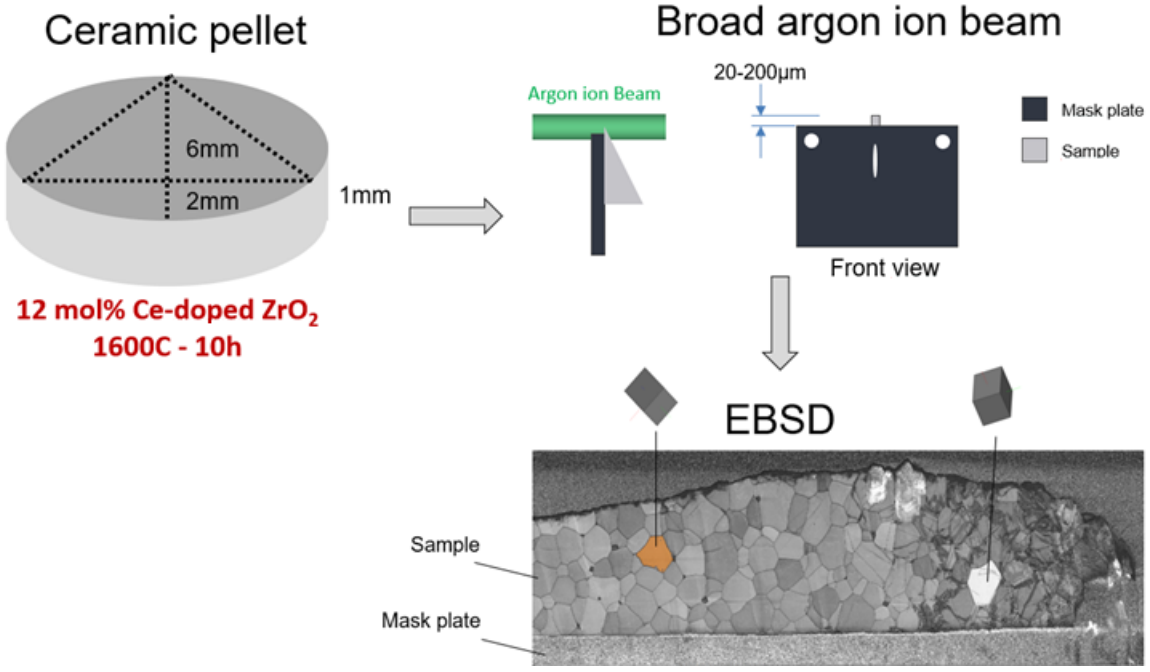

Figure 1 – Processing steps for micropillars processing, starting from bulk material, followed by broad beam polishing and EBSD grain selection previous to FIB milling.

During the deformation of ceria stabilized tetragonal zirconia, three deformation behaviors compete with each other: transformation, slip, and fracture. The martensitic transformation is likely to be affected by the crystal orientation[1]. The main criterium of the crystalline orientation of the grains selected for the preparation of the micropillars was the Schmid factor SF. For calculating SF, the tetragonal supercell faces ($\frac{c}{a} \approx 1$, $P\bar{4}m2$) were used as slip planes. After selecting the grains with crystalline orientations favoring the martensitic transformation, micropillars were milled out of the bulk material using a focused ion beam microscope (FIB, Zeiss NVision 40). In this experiment, two different pillar sizes were tested, one with an aspect ratio (height/diameter) around 2.5 - 3 ("P" pillars), and another with an aspect ratio around 4 ("C" pillars). The orientation for each P pillar is presented in the inverse pole figure displayed in Fig. 2 and Table 1. The Euler angles shown here are according to the primitive tetragonal unit cell ($P4_2/nmc$), to be comparable with the Laue microdiffraction indexation results. It is emphasized here that the relation between both cells is $[100]_{supercell}$ // $[110]_{primitive}$.

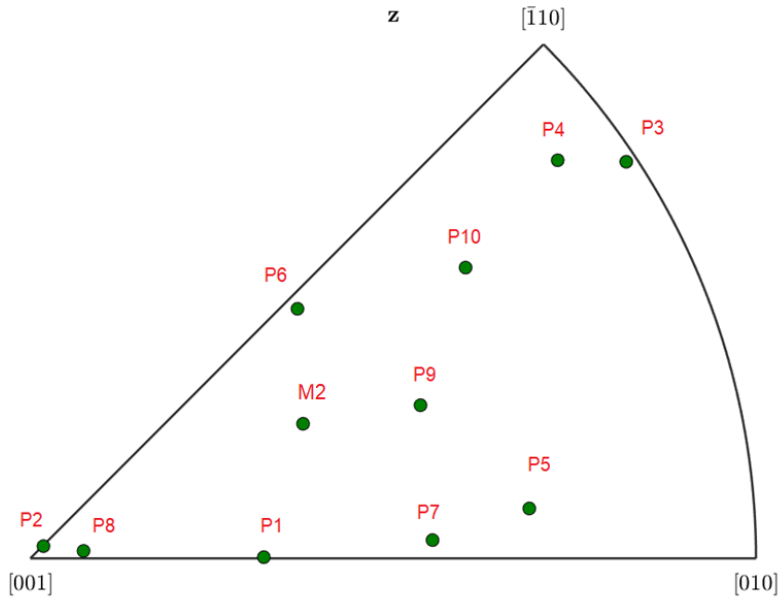

Figure 2 – Inverse pole figure exhibiting the orientations of the pillars processed for this experiment. Because of the different orientations, competition between fracture, slip, or transformation was expected.

Table 1 – Euler angles (E1, E2, E3) of pillars processed for the BM32 *in situ* compression experiment. Pillars noted as "P" had a starting tetragonal phase. Pillars M1 and M2 were completely and partially monoclinic, respectively. The Euler angles correspond to the primitive ($P4_2/nmc$) tetragonal phase orientation. The maximum Schmid factors (SF_{MAX}) were calculated based on the supercell configuration.

Pillar	E1	E2	E3	SF_{MAX}
P1	45.6	26.3	0.3	0.33
P2	81.9	2.0	47.0	0.08
P3	15.8	88.4	56.4	0.21
P4	142.4	80.1	53.0	0.21
P5	114.6	58.5	5.7	0.37
P6	120.7	138.3	47.0	0.50
P7	35.6	46.2	87.7	0.35
P8	127.5	6.0	82.0	0.08
P9	48.8	48.2	68.6	0.43
P10	5.8	61.3	33.7	0.38
M1	-	-	-	-
M2	175.8	144.8	65.3	0.44

For the other pillar configurations, their orientations are shown here according to their Miller indices in Table 2. Pillars C1 and C2 had already been compressed up to ~3.5 GPa and ~4.5 GPa, respectively. To illustrate how the pillars are aligned, a SEM image of the sample edge is shown in Fig. 3 for pillars P.

Table 2 – Miller indices of pillars processed for the BM32 *in situ* compression experiment. All pillars here started with a tetragonal phase. Notations "p" and "sp" mean respectively primitive and supercell. The maximum Schmid factors (SF_{MAX}) were calculated based on the supercell configuration.

Pillar	Orientation	SF_{MAX}
C1	$[110]_p//[100]_{sp}$	≈ 0
C2	$[001]$	≈ 0
C4	$[100]_p//[110]_{sp}$	≈ 0.5
C5	$[001]$	≈ 0

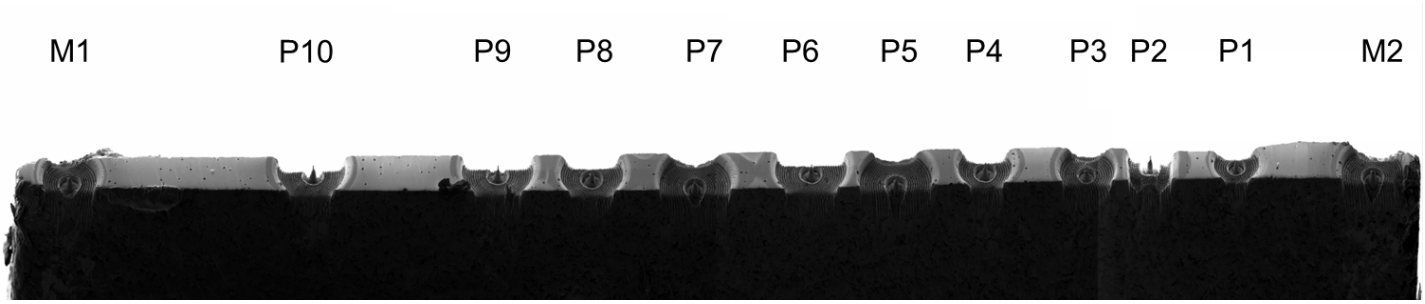

Figure 3 – Micropillars brought to the BM32 beamline for in situ compression.

For *in situ* microcompression tests, the nanoindenter FT-NMT04 (FemtoTools) equipped with a diamond flat punch was installed on the goniometer of the BM32 beamline. During compression in displacement-controlled mode with a displacement rate of 30 nm/s, Laue microdiffraction patterns were recorded using a sCMOS camera installed at 90° with respect to the incident polychromatic X-ray beam. Cyclic loading-unloading curves with increasing maximum load were applied to each micropillar until a clear load drop was visible in the load-displacement curve. 2D Laue microdiffraction maps were recorded of the micropillars both in their pristine state and after compression. The Laue microdiffraction patterns were indexed using the LaueTools software and the LaueTools neural network (newly developed by the BM32 beamline staff) which allowed to deduce the monoclinic and tetragonal crystalline phases, the crystalline orientation, and the deviatoric strain for each measurement position within the 2D Laue microdiffraction maps.

The calculated maximum stresses obtained from the load-dipalcement curves for all mechanically tested micropillars are shown in Fig. 4. It should be noted that pillars P3, P5, and P7 could not be precisely located, thus were not tested.

Due to a slight taper, the diameter of the micropillars increases from the top towards the bottom. The effecive diameter of the deformed zone was calculated[1] using Equation 1.

$$d_{eff} = \sqrt{\frac{1}{3}d_{top}^2 + d_{top}^2 d_{bot}^2 + d_{bot}^2} \quad (1)$$

Where d_{top} and d_{bot} are the top and bottom diameters of the transformed region, respectively.

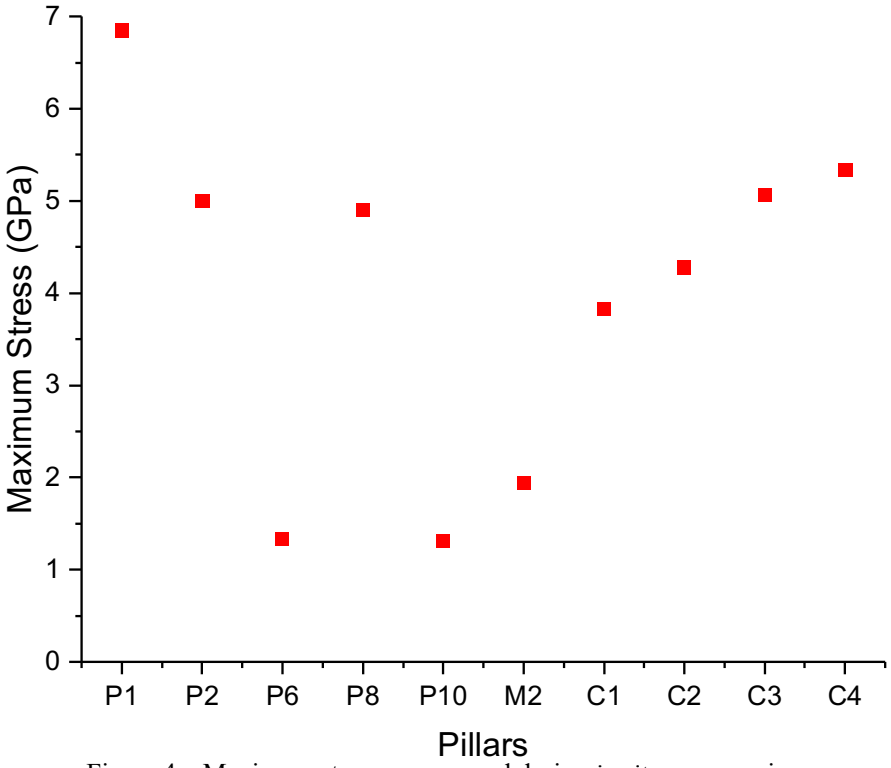

Figure 4 – Maximum stresses measured during *in situ* compression.

From Fig. 4, the maximum stresses calculated differ between the pillars due to their different orientations. For instance, pillars P2 and P8 (orientation ≈ [001]) exhibited a higher mechanical strength for inducing the transformation compared to pillars P6 and P10. This could be linked to the difference in Schmid factors. While the first two have a SF_{MAX} close to zero, the latter two are 0.38 and 0.50 respectively. In addition, for P1 even though the SF_{MAX} is 0.33, the maximum stress is the highest. Therefore, a more in-depth view of the mechanical behavior for transformation is needed. Scanning electron microcopy images and phase maps of the micropillar P6 before and after compression are presented in Fig. 5 together with the load-displacement curve showing a clearly visible load drop.

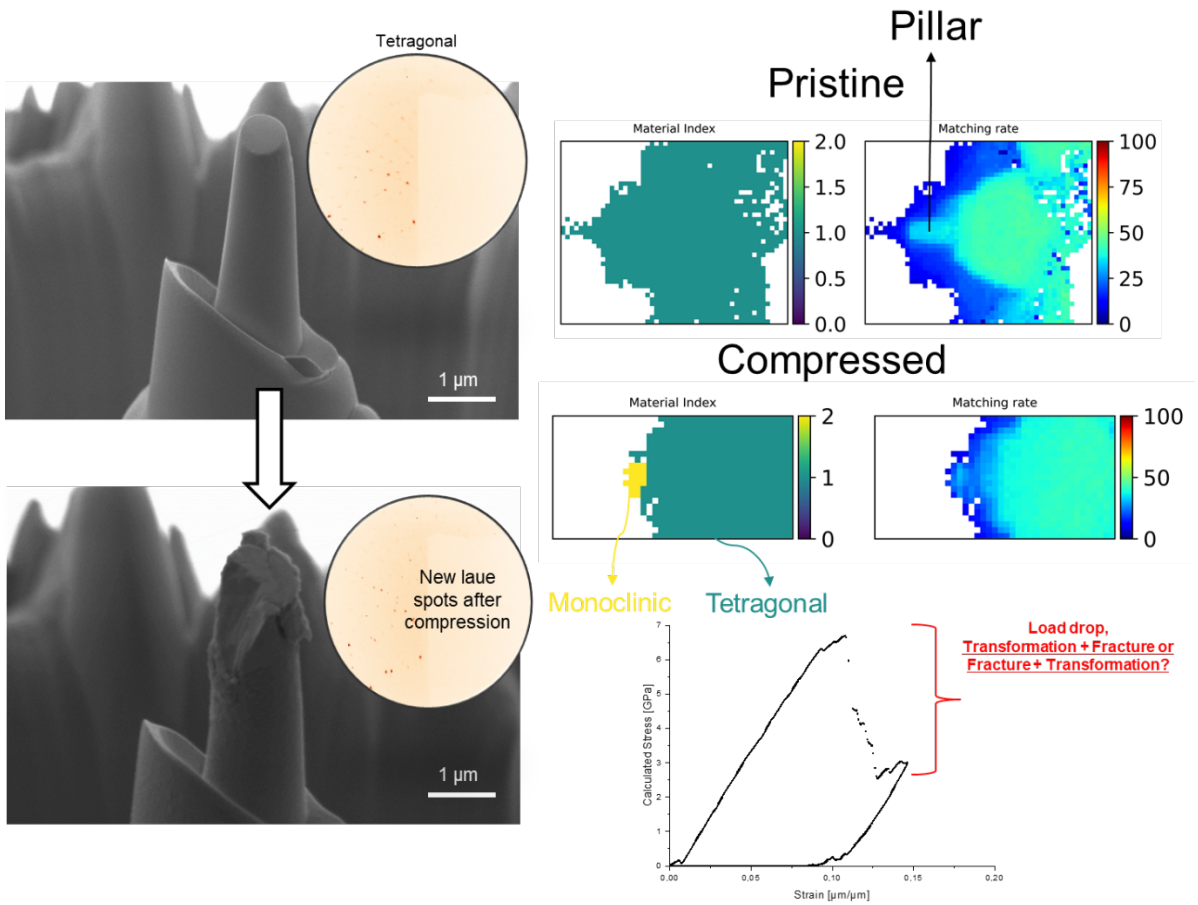

Figure 5 – Pristine and compressed state of pillar P1. The laue spot images were obtained using the lauetools software by using as input the data obtained during the experiment. The 2D maps were obtained using the lauetools neural network software, where the material index and matching rate are highlighted here. On the material index, green color means tetragonal phase, while yellow is monoclinic phase.

In Fig 5, the load drop can be observed around ~7 GPa. Analysing the material index map, it is clear that phase transformation was induced during the *in situ* compression test. Nevertheless, an important question that must be solved is if the transformation occurred before fracture, or the contrary. This is an important result, as it can lead us to better understand how the transformation onset, and can help in tailoring the materials properties in order to obtain transformation only, rather than fracture. Moreover, pillars where only transformation occurred were also observed, such as Pillar P6 (Fig. 9 in the annex).

From these preliminary results, the martensitic transformation was observed even for orientations that were believed to not favor the transformation, where the compression axis // crystal orientation. Some of the SEM images recorded after mechanical testing show cracks, raising the point of competition between transformation, slip, and fracture. If pillars "P" and "C" are compared, the latter presented higher maximum stresses. This can be related to the different aspect ratios and different crystalline orientations. In addition, misalignments may also affect the mechanical test, causing sample bending.

With this experiment, knowing the corresponding cell variant from the tetragonal→monoclinic transformation is possible, and will aid in understanding how the transformation is preferred for the 12 mol% ceria-doped zirconia. The next steps involve a time-resolved experiment to have a better resolution of when the transformation occurs along the stress-strain curve, and evaluation of by-crystalline micropillars to understand how the transformation propagates between grains.

References:

[1] Zeng, X. M., Lai, A., Gan, C. L., & Schuh, C. A. (2016). Crystal orientation dependence of the stress-induced martensitic transformation in zirconia-based shape memory ceramics. Acta Materialia, 116, 124–135.
[2] Micha, J.-S. & Robach, O., (2010). LaueTools laue x-ray microdiffraction analysis software.
[3] Purushottam Raj Purohit, R. R. P., Tardif, S., Castelnau, O., Eymery, J., Guinebretiere, R., Robach, O., Ors, T. & Micha, J.-S. (2022). J. Appl. Cryst. 55, 737-750.

Annex:

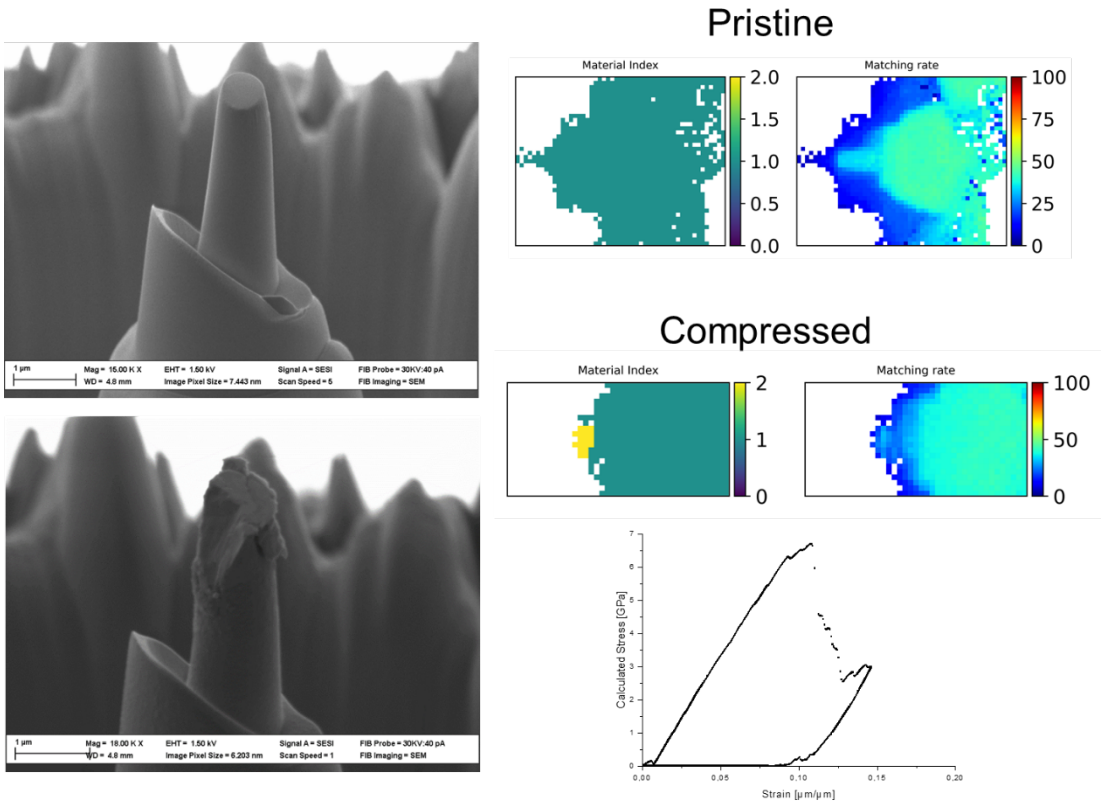

Figure 6 – Pillar P1 pristine and compressed state. Scanning electron microscope images, and laue maps acquired using lauenn are used here to represent the martensitic transformation. Because the machine is displacement-controlled, a load drop is observed during the transformation. From the material index map: green = tetragonal; yellow

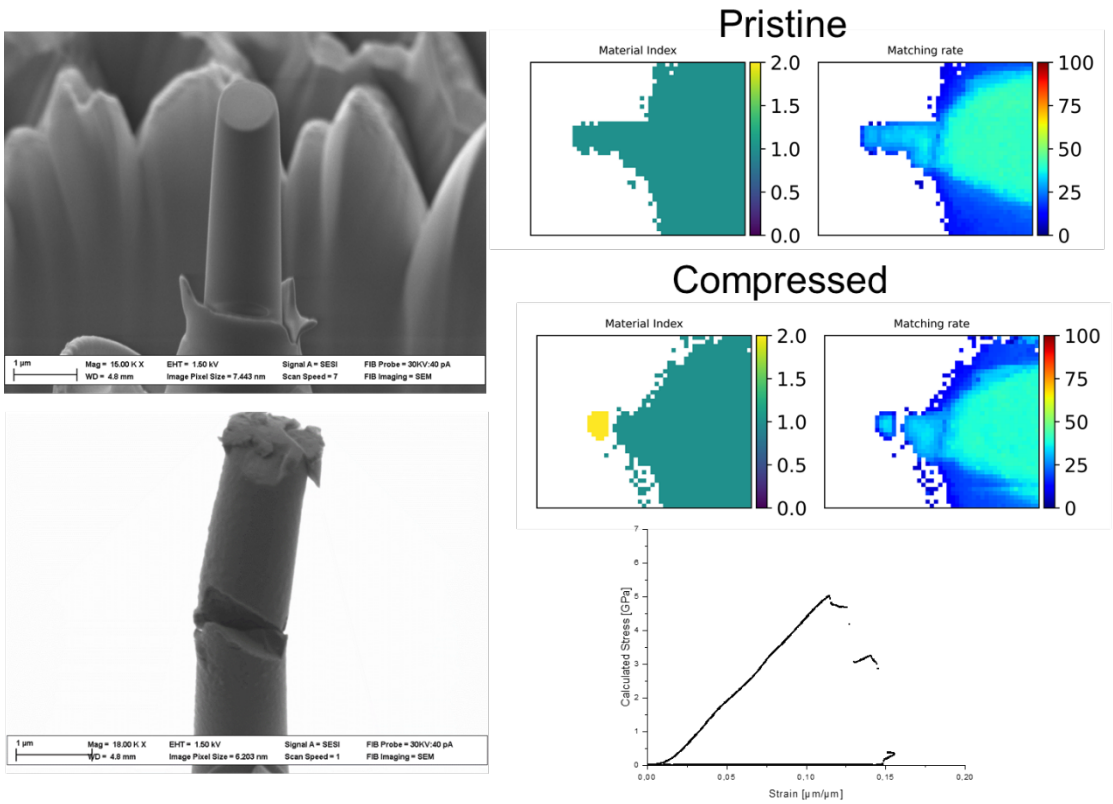

Figure 7 – Pillar P2 pristine and compressed state. Scanning electron microscope images, and laue maps acquired using lauenn are used here to represent the martensitic transformation. Because the machine is displacement-controlled, a load drop is observed during the transformation. From the material index map: green = tetragonal; yellow

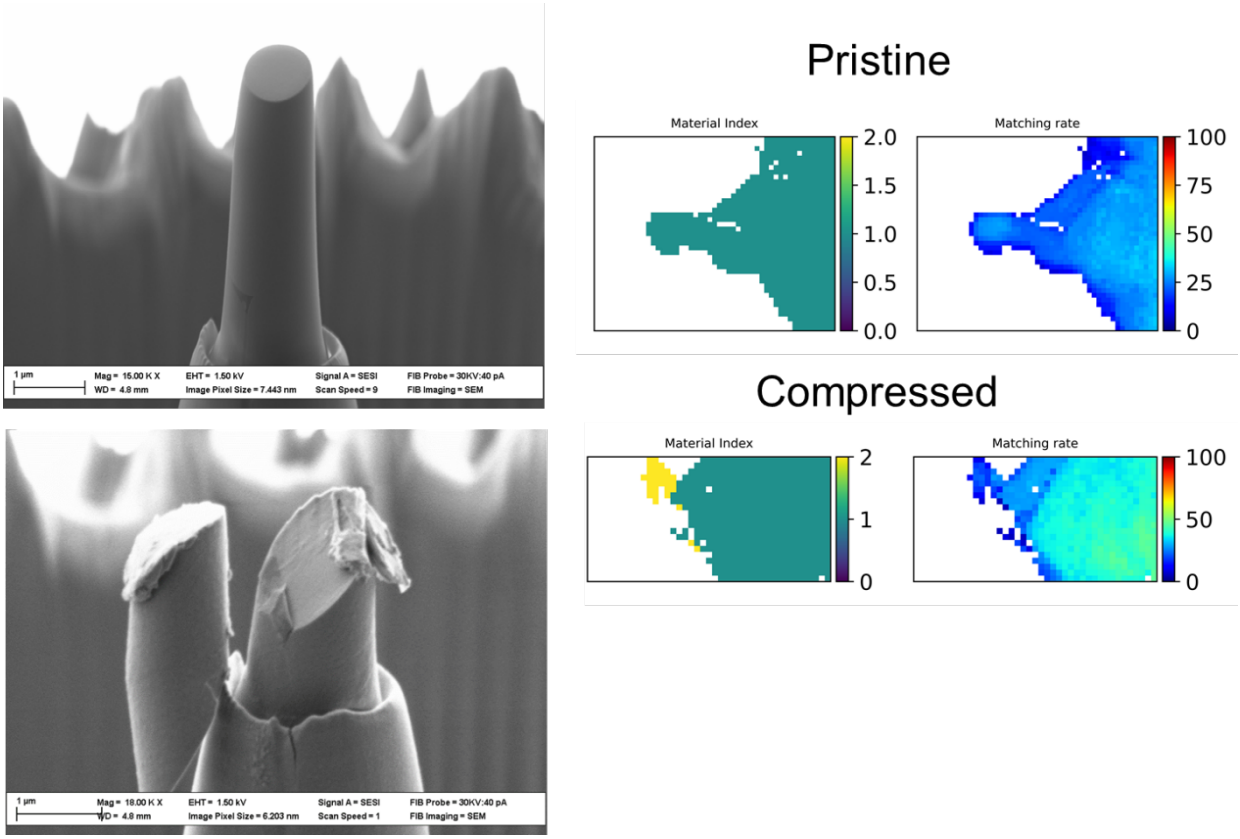

Figure 8 – Pillar P4 pristine and compressed state. Scanning electron microscope images, and laue maps acquired using lauenn are used here to represent the martensitic transformation. No mechanical data is available for this pillar. From the material index map: green = tetragonal; yellow

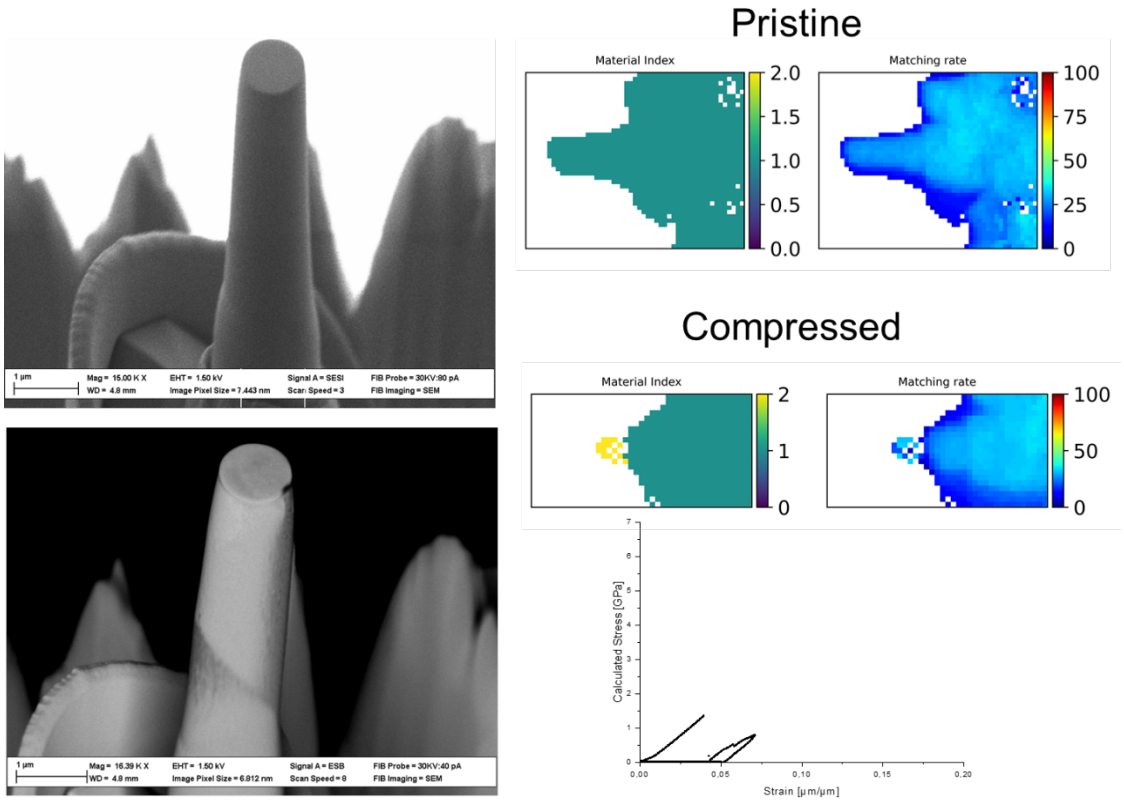

Figure 9 – Pillar P6 pristine and compressed state. Scanning electron microscope images, and laue maps acquired using lauenn are used here to represent the martensitic transformation. Because the machine is displacement-controlled, a load drop is observed during the transformation. From the material index map: green = tetragonal; yellow

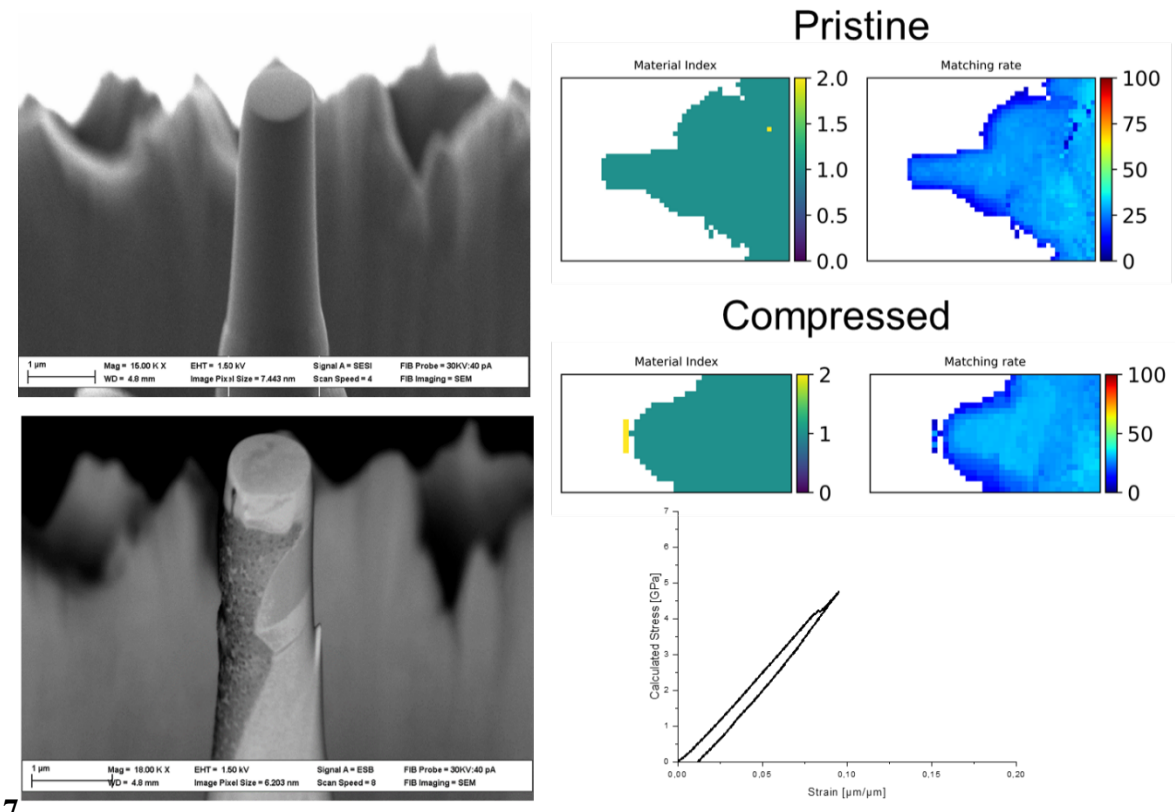

7

Figure 10 – Pillar P8 pristine and compressed state. Scanning electron microscope images, and laue maps acquired using lauenn are used here to represent the martensitic transformation. Because the machine is displacement-controlled, a load drop is observed during the transformation. From the material index map: green = tetragonal; yellow

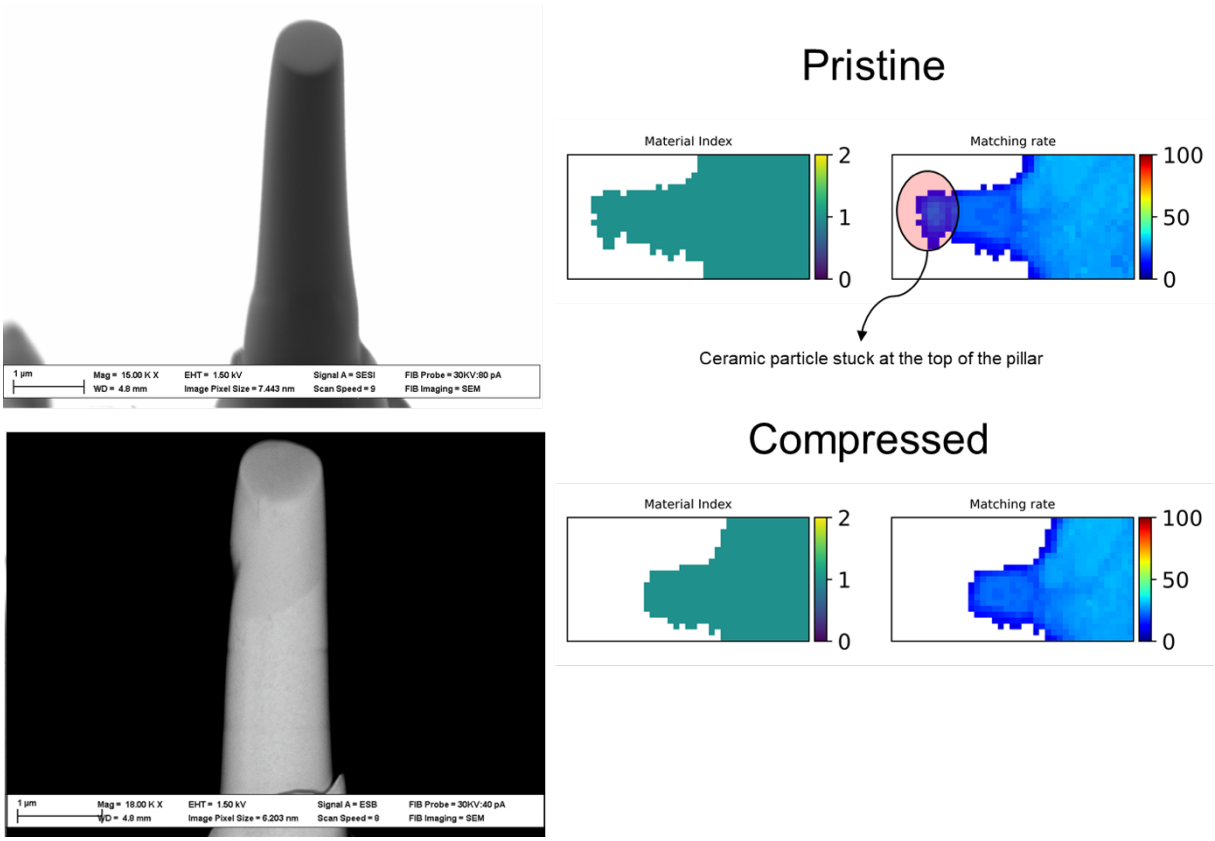

Figure 11 – Pillar P9 pristine and compressed state. Scanning electron microscope images, and laue maps acquired using lauenn are used here to represent the martensitic transformation. A zirconia particle was present during mechanical testing, thus the pillar was still considered undamaged and can be used for further mechanical tests. From the material index map: green = tetragonal; yellow

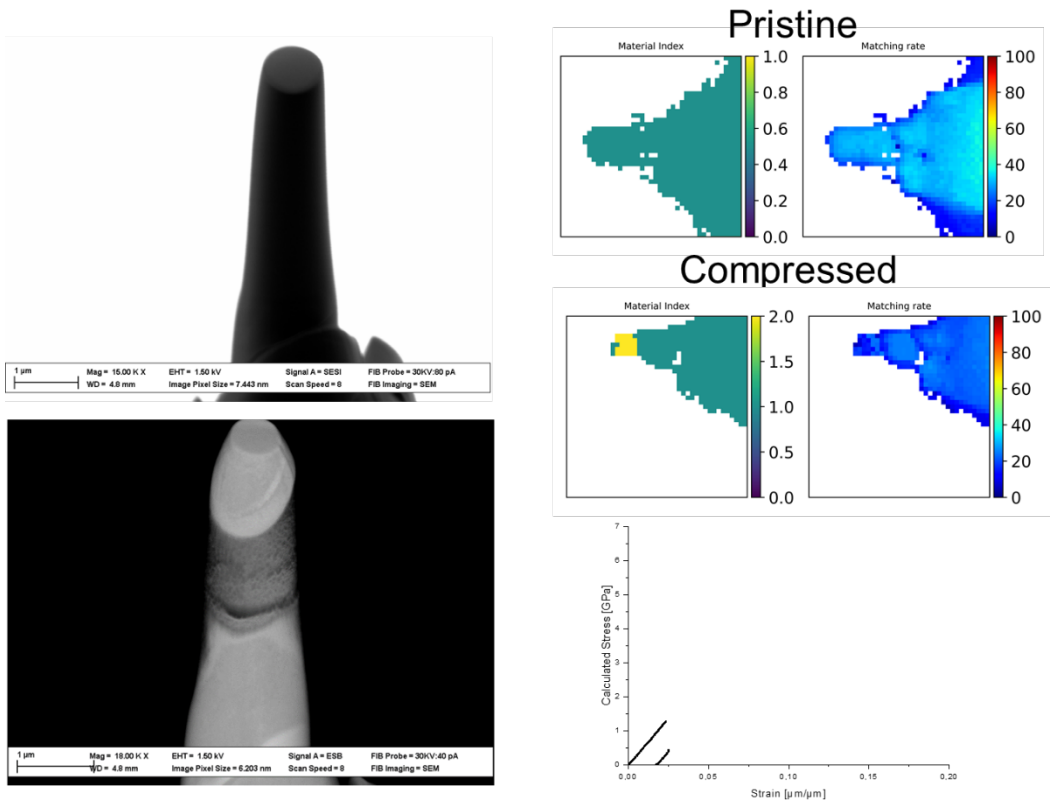

Figure 12 – Pillar P10 pristine and compressed state. Scanning electron microscope images, and laue maps acquired using lauenn are used here to represent the martensitic transformation. Because the machine is displacement-controlled, a load drop is observed during the transformation. From the material index map: green = tetragonal; yellow

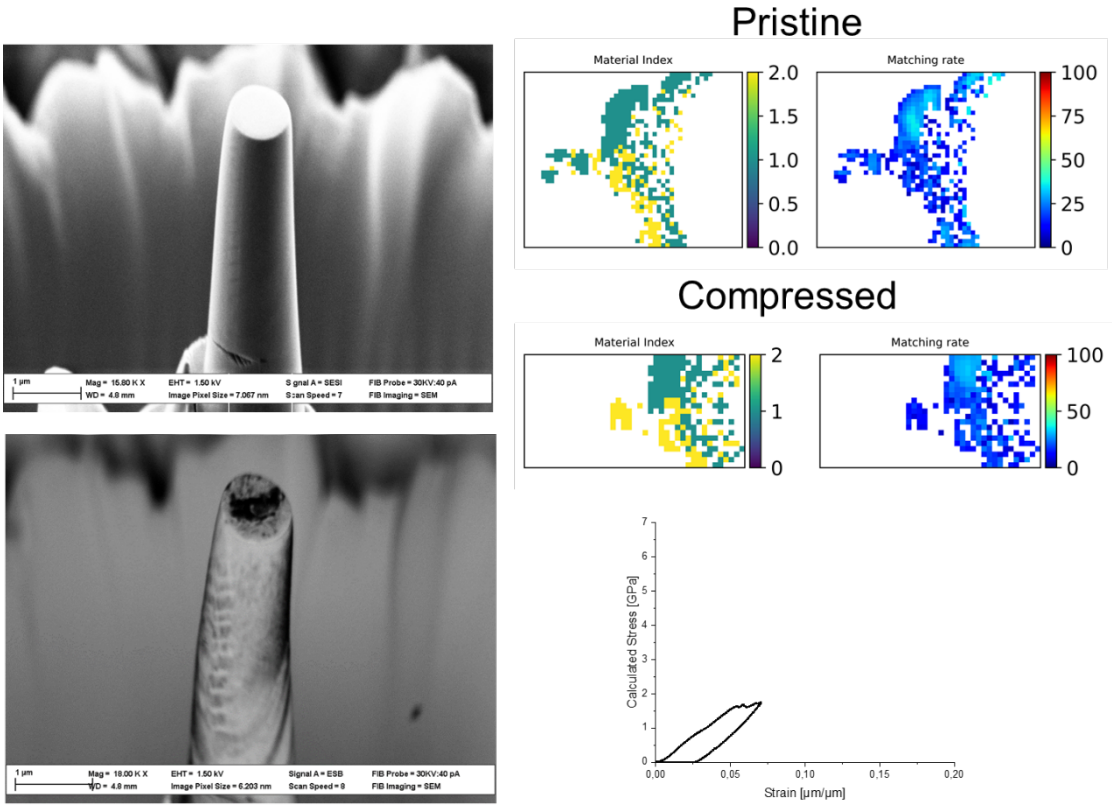

Figure 13 – Pillar M2 pristine and compressed state. Scanning electron microscope images, and laue maps acquired using lauenn are used here to represent the martensitic transformation. Because this pillar was partially transformed in its pristine state, the stress-strain curve does not present sudden changes like other pillars. Rather, the transformation seems more moderate, translating in smaller load drops. From the material index map: green = tetragonal; yellow

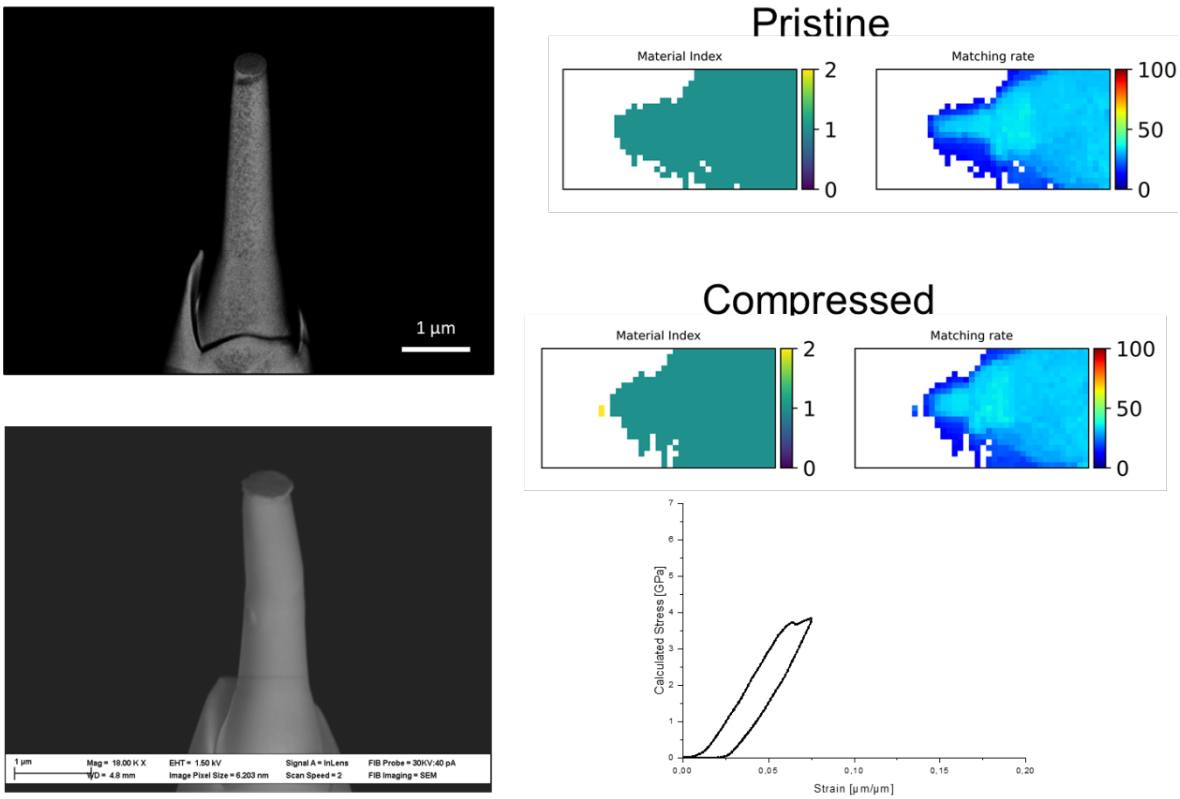

Figure 14 – Pillar C1 pristine and compressed state. Scanning electron microscope images, and laue maps acquired using lauenn are used here to represent the martensitic transformation. From the material index map: green = tetragonal; yellow

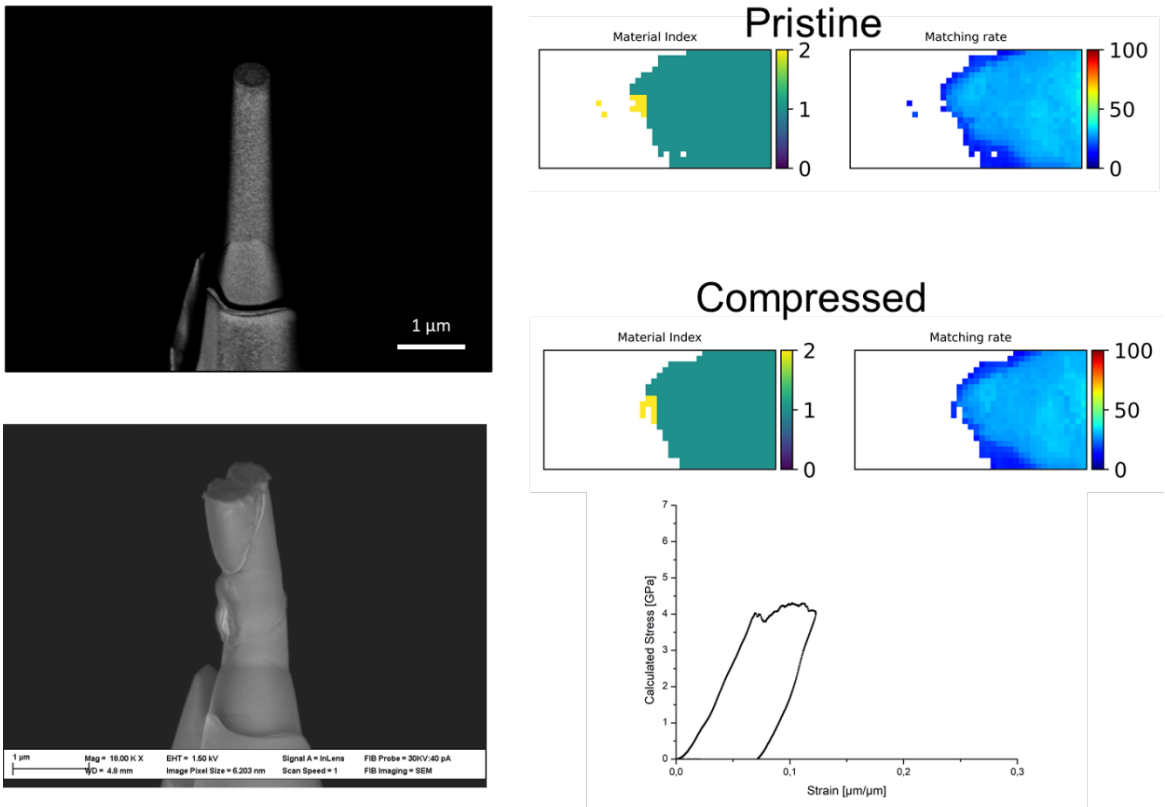

Figure 15 – Pillar C2 pristine and compressed state. Scanning electron microscope images, and laue maps acquired using lauenn are used here to represent the martensitic transformation. From the material index map: green = tetragonal; yellow

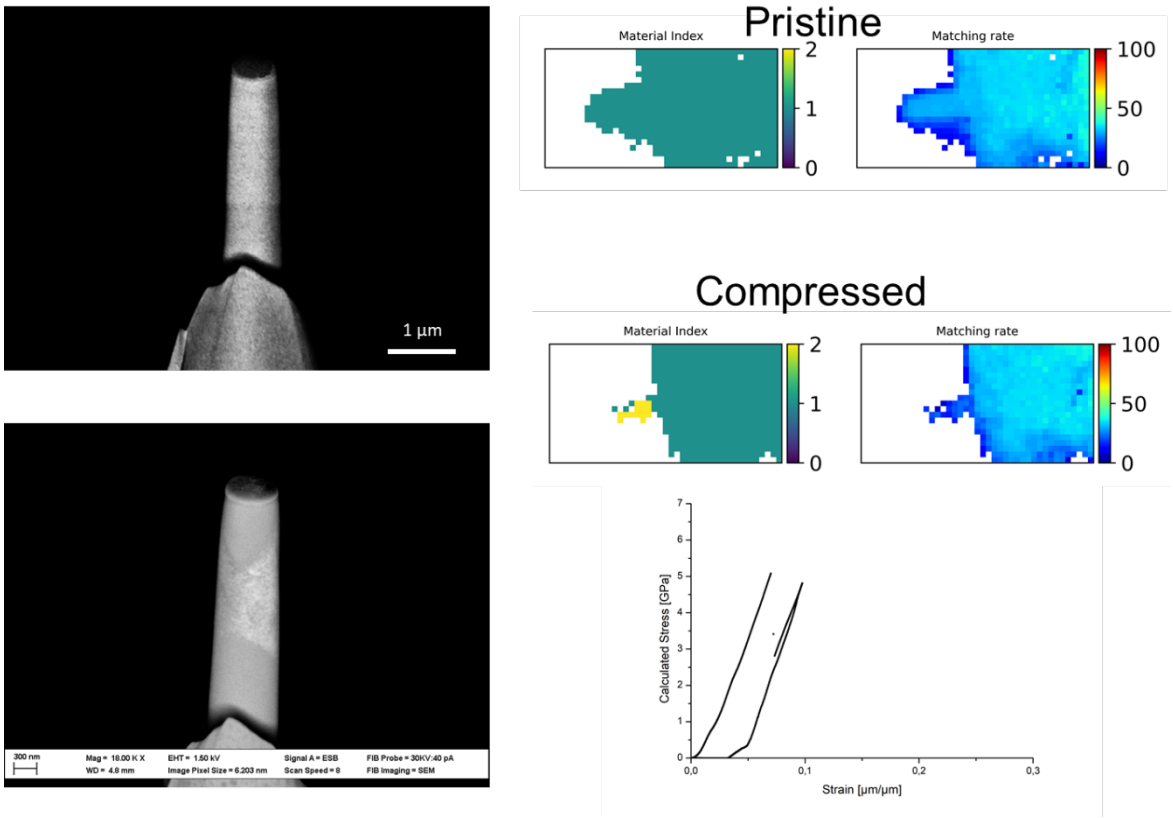

Figure 16 – Pillar C4 pristine and compressed state. Scanning electron microscope images, and laue maps acquired using lauenn are used here to represent the martensitic transformation. From the material index map: green = tetragonal; yellow

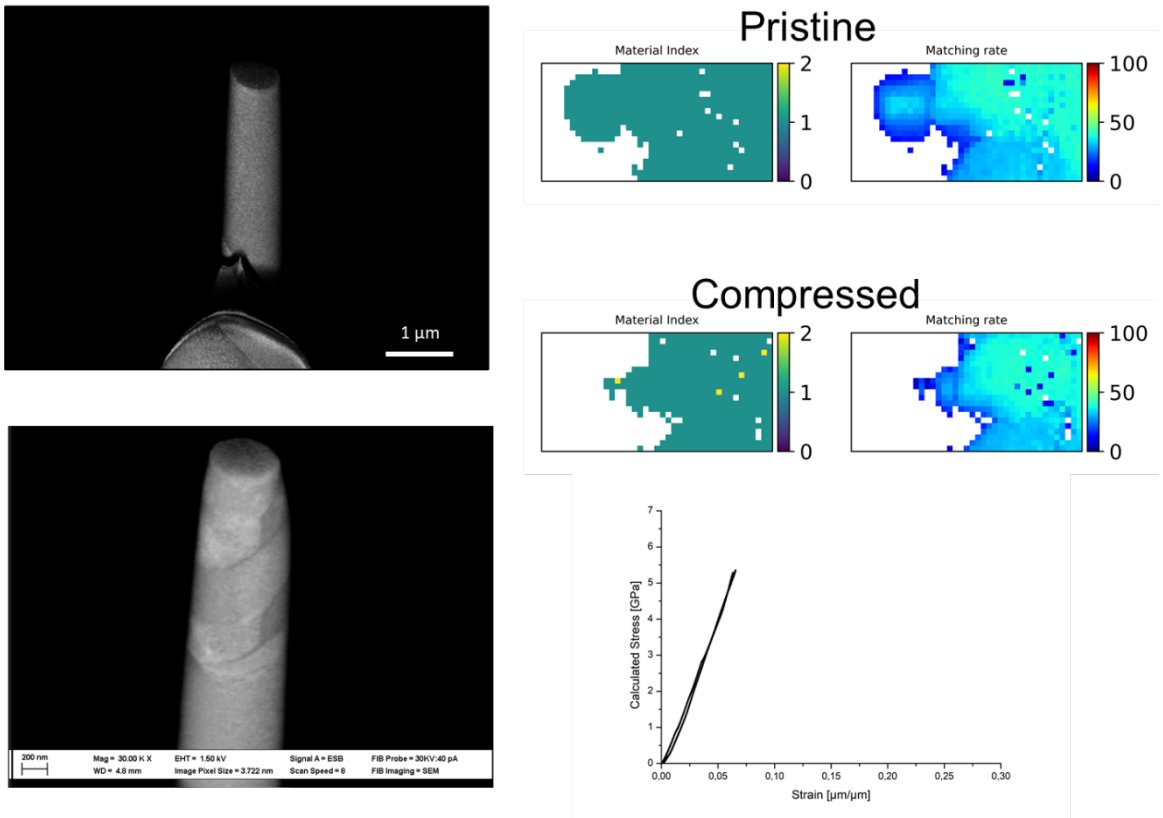

Figure 17 – Pillar C5 pristine and compressed state. Scanning electron microscope images, and laue maps acquired using lauenn are used here to represent the martensitic transformation. From the material index map: green = tetragonal; yellow